Numerical simulations of plasma sheaths

Valentin Ayot[*], Mehdi Badsi[†], Yann Barsamian, Anaïs Crestetto[‡], Nicolas Crouseilles[§], Michel Mehrenberger[¶], Averil Prost[‖], Christian Tayou-Fotso[**]

Centre de Calcul Intensif d'Aix-Marseille is acknowledged for granting access to its high performance computing resources

Abstract

This article is a report of the CEMRACS 2022 project, called HIVLASHEA, standing for "**Hi**gh order methods for **Vla**sov-Poisson models for **shea**ths". A two-species Vlasov-Poisson model is described together with some numerical simulations, permitting to exhibit the formation of a plasma sheath. The numerical simulations are performed with two different methods: a first order classical finite difference (FD) scheme and a high order semi-Lagrangian (SL) scheme with Strang splitting; for the latter one, the implementation of (non-periodic) boundary conditions is discussed. The codes are first evaluated on a one-species case, where an analytical solution is known. For the two-species case, cross comparisons and the influence of the numerical parameters for the SL method are performed in order to have an idea of a reference numerical simulation.

1 Introduction

Plasmas are neutral at the equilibrium in a sufficiently large domain. However, near a boundary, a charge imbalance may be observed in a thin layer called *sheath*. This phenomenon stems from the interaction of ions and electron with the boundary media (a cold metallic wall, for instance). Both species will be absorbed by the wall, but with a rate proportional to their speed. Since the electrons are moving faster than the ions, a positively charged layer (the *Debye sheath*) forms near the boundary.

Plasma sheaths are particularly challenging to simulate, as we have to deal with different scales. and in this region, the plasma parameters (temperature or density) develop steep gradients. Due to their different mass, electrons and ions have a very different behavior close to the boundary, a two-species model is required to describe the formation of the sheath. Moreover, kinetic models are necessary to capture the velocity effect of the particles [BMG$^+$]. Hence, we are considering in this work a two-species Vlasov model to run simulations of the plasma sheath.

Recent works are dedicated to the non homogeneous equilibrium sheath, both on the mathematical side and on the numerical side [**?**, BBC21, **?**]. Regarding the dynamical approaches, one refer to [**?**, BMG$^+$] or [BMN] for which this study is a follow-up. In the latter work, we studied the behavior of the numerical solution of the Vlasov equation, initialized with a sheath homogeneous equilibrium. In this work, our purpose

[*]Institut de Mathématiques, CNRS, UMR 5251, Université de Bordeaux, F-33405 Talence, France. valentin.ayot@u-bordeaux.fr

[†]Nantes Université, Laboratoire de Mathématiques Jean Leray, 2 Chemin de la Houssinière BP 92208, 44322 Nantes Cedex 3

[‡]Nantes Université, Laboratoire de Mathématiques Jean Leray, 2 Chemin de la Houssinière BP 92208, 44322 Nantes Cedex 3

[§]Univ Rennes, Inria (Mingus team), IRMAR UMR 6625 and ENS Rennes, France. nicolas.crouseilles@inria.fr

[¶]I2M, CMI, UMR 7373, 39 rue Frédéric Joliot Curie, 13453 Marseille Cedex 13

[‖]INSA de Rouen, LMI (EA 3226 - FR CNRS 3335), 685 Avenue de l'Université, 76801 St Etienne du Rouvray cedex, France. averil.prost@insa-rouen.fr

[**]Labo. J. A. Dieudonné, UMR 6621, Université Nice-Sophia Antipolis, Parc Valrose, F-06108 Nice cedex 02, France. christian.tayou-fotso@unice.fr

is to investigate numerically the formation of a sheath, when we include ionization in the model, inspired by the recent work [**?**] where a fluid model is proposed.

Then, we are concerned by the numerical approximation of the two-species Vlasov model including ionization and boundary. To do so, we propose a high order semi-Lagrangian method combined with a time splitting method. The presence of boundaries requires specific adaptation to define correctly the semi-Lagrangian method close to the boundary. We adapt the strategies developed in [CL20, **?**] to define inflow and outflow ghost points according to the order of the Lagrange interpolation used in the semi-Lagrangian method.

The rest of the work is organized as follows: In Section 2, we introduce the two-species Vlasov-Poisson system with boundary, the numerical methods are described in Section 3 and numerical results are given in Section 4.

2 Plasma sheaths

The model Let $t \in \mathbb{R}^+$ denote the time variable, $x \in [-1,1]$ denote the spatial variable in a normalized one-dimensional domain, and $v \in \mathbb{R}$ denote the speed variable. The distribution of species is described through their density in the phase space, denoted by $f_i : (t,x,v) \in \mathbb{R}^+ \times [-1,1] \times \mathbb{R} \mapsto \mathbb{R}$ for the ions, and $f_e : (t,x,v) \in \mathbb{R}^+ \times [-1,1] \times \mathbb{R} \mapsto \mathbb{R}$ for the electrons. To these kinetic quantities, we add the spatial densities $n_{i,e}$ and currents $J_{i,e}$, defined by

$$n_{i,e}(t,x) \coloneqq \int_{v\in\mathbb{R}} f_{i,e}(t,x,v)dv, \quad \text{and} \quad J_{i,e}(t,x) \coloneqq \int_{v\in\mathbb{R}} v f_{i,e}(t,x,v)dv. \tag{2.1}$$

In the sequel, we will denote $n(t,x) \coloneqq n_i(t,x) - n_e(t,x)$, and $J(t,x) \coloneqq J_i(t,x) - J_e(t,x)$.

The evolution of the densities is modelled by the Vlasov-Poisson equations. Let $\varphi : \mathbb{R}^+ \times [-1,1] \mapsto \mathbb{R}$ denote the electric potential, then we consider the following model satisfied by (f_e, f_e, φ)

$$\begin{cases} \partial_t f_i + v\partial_x f_i - \partial_x\varphi\, \partial_v f_i = \nu f_e, & (t,x,v) \in \mathbb{R}_*^+ \times]-1,1[\times\mathbb{R}, & \text{(2.2a)} \\ \partial_t f_e + v\partial_x f_e + \dfrac{\partial_x\varphi}{\mu}\, \partial_v f_e = 0, & (t,x,v) \in \mathbb{R}_*^+ \times]-1,1[\times\mathbb{R}, & \text{(2.2b)} \\ -\lambda^2\partial_{xx}^2\varphi = n(t,x), & (t,x) \in \mathbb{R}^+ \times]-1,1[. & \text{(2.2c)} \end{cases}$$

The physical parameters ν, μ and λ have the following meaning:

- $\nu \geqslant 0$ is the ionization frequency. It describes the rate of creation of ions in presence of electrons.
- $\mu \coloneqq m_e/m_i$ is the mass ratio between electrons and ions.
- $\lambda > 0$ is the Debye length.

In the sequel, we may use the electric field $E(t,x) \coloneqq -\partial_x\varphi(t,x)$ in place of the potential. Then, the second-order Poisson equation rewrites as

$$\lambda^2\partial_x E(t,x) = n(t,x), \qquad (t,x) \in \mathbb{R}^+ \times]-1,1[. \tag{2.3}$$

Remark 2.1. *To reduce the notations, we will use f_s, $s \in \{i,e\}$ to denote both the electronic and ionic distributions. The Vlasov equations* (2.2a) *and* (2.2b) *rewrite*

$$\partial f_s + v\partial_x f_s - c_s\partial_x\varphi\partial_v f_s = S_s,$$

with the coefficients c_s and source terms S_s defined as

$$c_i \coloneqq 1, \quad c_e \coloneqq -\frac{1}{\mu}, \quad S_i \coloneqq \nu f_e, \quad S_e \coloneqq 0.$$

The densities f_i and f_e are subject to initial and boundary conditions, given by

$$\begin{cases} f_s(0,x,v) \coloneqq f_s^0(x,v), & (x,v) \in]-1,1[\times\mathbb{R}, \quad (2.4a) \\ f_s(t,x=\pm 1,\pm v<0) \coloneqq 0, & t \in \mathbb{R}_*^+. \quad (2.4b) \end{cases}$$

The homogeneous boundary condition (2.4b) stems from the non-emitting wall model: the boundary absorbs particles without any reflection. This loss of particles is compensated by the ionization source term in the right hand side of (2.2a).

To completely describe the model, we still need to provide boundary conditions for the Poisson problem (2.2c). A first one is given by the choice of a reference potential

$$\varphi(t,0) = 0 \qquad \forall t \in \mathbb{R}^+. \tag{2.5}$$

To derive a second boundary condition, we introduce a fundamental symmetry assumption.

Symmetry We will look for *symmetric solutions* for 2.2, ie solutions satisfying

$$\varphi(t,x) = \varphi(t,-x) \qquad (t,x) \in \mathbb{R}^+ \times [-1,1]. \tag{2.6}$$

By derivation with respect to $x \in]-1,1[$, we immediately obtain

$$\partial_x\varphi(t,x) = -\partial_x\varphi(t,-x), \quad \text{i.e.} \quad E(t,x) = -E(t,-x).$$

In particular, the electric field vanishes at $x=0$, and the Neumann boundary condition

$$\partial_x\varphi(t,0) = 0 \quad \text{or equivalently} \quad E(t,0) = 0 \tag{2.7}$$

may be used (with (2.5)) to close the Poisson equation (2.2c).

Let us notice that the Vlasov equations (2.2a) and (2.2b) are driven by the vector fields

$$(t,x,v) \to (1,v,E(t,x)) =: V_i(t,x,v) \quad \text{and} \quad (t,x,v) \to (1,v,-E(t,x)/\mu) =: V_e(t,x,v).$$

Both these fields satisfy the radial symmetry $V_s(t,x,v) = V_s(t,-x,-v)$. In consequence, if we assume that $f_s^0(x,v) = f_s^0(-x,-v)$, the solutions $f_s(t,x,v)$ will be radially symmetric around $(t,0,0)$, i.e.

$$f_i(t,x,v) = f_i(t,-x,-v) \quad \text{and} \quad f_e(t,x,v) = f_e(t,-x,-v) \quad \forall (t,x,v) \in \mathbb{R}^+ \times [-1,1] \times \mathbb{R}.$$

In particular, we have for the densities and currents

$$\begin{aligned} n_s(t,x) &= \int_{v\in\mathbb{R}} f_s(t,x,v)dv = \int_{w\in\mathbb{R}} f_s(t,x,-w)dw = \int_{w\in\mathbb{R}} f_s(t,-x,w)dw = n_s(t,-x), \\ J_s(t,x) &= \int_{v\in\mathbb{R}} v f_s(t,x,v)dv = -\int_{w\in\mathbb{R}} w f_s(t,x,-w)dw = -\int_{w\in\mathbb{R}} w f_s(t,-x,w)dw = -J_s(t,-x). \end{aligned}$$

Remark 2.2 (Additional symmetry of f_e)**.** *Notice that the function $f : (t,x,v) \to f_e(t,x,v) - f_e(t,x,-v)$ satisfies the linear equation*

$$0 = \partial_t f(t,x,v) + v\partial_x f(t,x,v) - \frac{E(t,x)}{\mu}\partial_v f(t,x,v).$$

The boundary condition (2.4b) *gives $f(t,\pm 1,\pm v<0) = 0$. If, in addition, we assume that the initial condition f_e^0 satisfies $f_e^0(x,v) - f_e^0(x,-v) = 0$, then we obtain*

$$f_e(t,x,v) = f_e(t,x,-v) \quad \forall (t,x,v) \in \mathbb{R}^+ \times [-1,1] \times \mathbb{R}. \tag{2.8}$$

Deriving a boundary condition at $x = \pm 1$ The centered Neumann condition (2.7) enforces continuity of $\partial_x \varphi$ at $x = 0$. We may avoid this constraint by deriving another Neumann condition, given on the boundary $x = \pm 1$.

First, we derive with respect to time the Poisson equation (2.2c)

$$-\partial_t(\lambda^2 \partial_{xx}^2 \varphi) = \partial_t n,$$

and considering the difference between the v-integration of the Vlasov equations (2.2a) and (2.2b) gives (recalling $n = n_i - n_e$ and $J = J_i - J_e$)

$$\partial_t n = \nu n_e - \partial_x J,$$

leads to (using $E = -\partial_x \varphi$)

$$\partial_x(\lambda^2 \partial_t E + J) = \nu n_e, \quad \forall x \in]-1, 1[.$$

Integrating now in space $x \in\in [-1, 1]$ leads to

$$\lambda^2 \partial_t E(t, 1) + J(t, 1) = \lambda^2 \partial_t E(t, -1) + J(t, -1) + \nu \int_{-1}^{1} n_e(t, x) dx, \tag{2.9}$$

and using the symmetries $E(t, 1) = -E(t, -1)$ and $J(t, 1) = -J(t, -1)$, it comes

$$\lambda^2 \partial_t E(t, \pm 1) + J(t, \pm 1) = \pm \frac{\nu}{2} \int_{-1}^{1} n_e(t, x) dx. \tag{2.10}$$

Time integration gives a condition of the form $E(t, \pm 1) = C_\pm(t)$, where

$$E(t, \pm 1) = C_\pm(t) \coloneqq E(0, \pm 1) - \frac{1}{\lambda^2} \int_0^t J(s, \pm 1) ds \pm \frac{\nu}{2\lambda^2} \int_0^t \int_{-1}^{1} n_e(s, x) dx ds. \tag{2.11}$$

NC : ne vaut-il pas mieux definir la constante par rapport au champ E plutot que par rapport au potentiel φ dont on ne sert plus ?

3 Numerical methods

In this section, the numerical methods used to approximate the system 2.2 are described. First, we focis on the Poisson equation and then, two numerical methods are presented for the Vlasov part.

3.1 Poisson equation

First, we focus on the approximation of the Poisson equation 2.2c The Poisson problem is solved with integral representations of the variable E.

First, we consider the centered Neumann boundary condition (2.7). Then, integrating the Poisson problem (2.3) over $[0, x]$ yields

$$E(t, x) = 0 + \int_0^x n(t, y) dy = \int_0^x \int_{v \in \mathbb{R}} [f_i(t, y, v) - f_e(t, y, v)] dv dy. \tag{3.1}$$

Let us now consider the boundary condition 2.11. The spatial domain $[-1, 1]$ is split into its positive and negative part, and integrating (2.3) gives

$$E(t, x) = \begin{cases} E(t, \quad 1) - \int_x^1 n(t, y) dy = C_+(t) - \int_x^1 \int_{v \in \mathbb{R}} [f_i(t, y, v) - f_e(t, y, v)] dv dy & x \in [0, 1] \\ E(t, -1) + \int_{-1}^x n(t, y) dy = C_-(t) + \int_{-1}^x \int_{v \in \mathbb{R}} [f_i(t, y, v) - f_e(t, y, v)] dv dy & x \in [-1, 0[\end{cases} \tag{3.2}$$

Note that here, the electric field may "jump" at $x = 0$. Both expressions may be approximated by quadrature formulas.

3.2 Finite Differences (FD)

Define a numerical computation domain $\Omega \coloneqq [-1,1] \times [-\overline{V},\overline{V}]$, with a large enough maximum speed $\overline{V}$. Let $(x_j, v_k)_{k\in[\![0,K]\!]}^{j\in[\![0,J]\!]}$ be a cartesian grid of Ω of step $(\Delta x, \Delta v)$. We discretize the advection equations on the subgrid $(x_j, v_k)_{k\in[\![1,K-1]\!]}^{j\in[\![1,J-1]\!]}$ by an explicit Euler scheme in time, and the upwind scheme in space:

$$\frac{f_{s,j,k}^{n+1} - f_{s,j,k}^{n}}{\Delta t} + D_{j,k}^{-} f_s^n \begin{pmatrix} v_k \\ c_s E_j^n \end{pmatrix}_+ + D_{j,k}^{+} f_s^n \begin{pmatrix} v_k \\ c_s E_j^n \end{pmatrix}_- = S_{s,j,k}^n, \tag{3.3}$$

where $a_+ = \max(a,0)$ and $a_- = \min(a,0)$ are respectively the pointwise positive and negative parts, and the uncentered finite differences are defined as

$$D_{j,k}^{\pm} f \coloneqq \pm \left(\frac{f_{j\pm1,k} - f_{j,k}}{\Delta x}, \frac{f_{j,k\pm1} - f_{j,k}}{\Delta v} \right).$$

The values of $f_{s,j,k}^n$ on the boundary ($j = 0, J$ and $k = 0, K$) are taken as follows:

- the boundary condition (2.4b) yields $f_{s,j,k}^n = 0$ whenever $x_j = -1, v_k > 0$ or $x_j = 1, v_k < 0$.
- it is considered that $\overline{V}$ is large enough to take the values on the speed boundary $v_k = \pm\overline{V}$ equal to 0.
- the remaining values $f_{s,j,k}^n$, $x_j = -1, -\overline{V} < v_k \leqslant 0$ or $x_j = 1, 0 \leqslant v_k < \overline{V}$ may be computed using the scheme (3.3), since the sign of the speed allows to use only inner points.

The upwind scheme is known to be diffusive, and stable under the CFL condition

$$1 - \max_k |v_k| \frac{\Delta t}{\Delta x} - |c_s| \max_j |E_j^n| \frac{\Delta t}{\Delta v} \geqslant 0 \quad \forall s \in \{i,e\} \text{ and } n \in [\![1,N]\!].$$

Given Δx and Δv, we deduce a sufficiently small value of Δt with the bound

$$\Delta t \leqslant \min\left(\frac{\Delta x}{\overline{V}}, \min(1,\mu) \frac{\Delta v}{E_{\max}} \right), \quad E_{\max} > 0 \text{ postulated } \textit{a priori}.$$

3.3 Semi-Lagrangian (SL)

The full model (2.2) nicely lends itself to approximation by time splitting. Indeed, consider the following Strang splitting decomposition

$$\begin{array}{ll}
\dfrac{\Delta t}{2} & \begin{cases} \partial_t f_s + v \partial_x f_s = 0 & \text{Linear advection along } x, \\ \lambda^2 \partial_x E = n_i - n_e & \text{Poisson problem,} \end{cases} \\
\dfrac{\Delta t}{2} & \partial_t f_i = \nu f_e \qquad \text{Ionization,} \\
\Delta t & \partial_t f_s + c_s E \partial_v f_s = 0 \quad \text{Linear advection along } v, \\
\dfrac{\Delta t}{2} & \partial_t f_i = \nu f_e \qquad \text{Ionization,} \\
\dfrac{\Delta t}{2} & \begin{cases} \lambda^2 \partial_x E = n_i - n_e & \text{Poisson problem,} \\ \partial_t f_s + v \partial_x f_s = 0 & \text{Linear advection along } x. \end{cases}
\end{array}$$

Each of the splitting step may be solved exactly (NC: pas vraiment "exactly" à cause des conditions aux bords $C_\pm$ qui font intervenir des intégrales en temps ; on avait construit une méthode de type trapèze en temps pour cela qu'on pourrait écrire). Indeed, the Poisson problems are solved by the integral representations (3.1) and (3.2). The ionization steps are pointwise ODE with time-independant source term, and are exactly solved by the explicit Euler scheme. Finally, notice that each advection is at constant speed with respect to the advection variable. This allows for the use of elementary 1D solvers.

Numerical treatment of the boundaries Let us focus on the elementary advection equation with constant speed $a > 0$

$$\partial_t f(t,x) + a\partial_x f(t,x) = 0, \quad f(t,-1) = 0, \quad \forall (t,x) \in \mathbb{R}_*^+ \times]-1,1[.$$

Let $(x_j)_{j\in[\![0,J]\!]}$ be a space mesh of step $\Delta x \coloneqq 2/J$, and $(t_n)_{n\in[\![0,N]\!]}$ be a time mesh of step $\Delta t \coloneqq T/N$. We follow the work of [CL20, **?**], and consider a semi-Lagrangian scheme defined as

$$f_j^{n+1} = \text{Lagrange interpolation}\,(f^n, x_j - a\Delta t) \coloneqq \sum_{k=-d}^{d+1} f_{j_0+k}^n L_k(\alpha),$$

with $(L_k)_{k\in[\![-d,d+1]\!]}$ the Lagrange polynomes of degree $(2d+1)$ defined by $L_k(z) = \prod_{\ell=-d,\ell\neq k}^{d+1} \frac{z-k}{\ell-k}$ (which satisfy $L_k(\ell) = \delta_{k\ell}$ for $\ell \in [\![-d, d+1]\!]$), and $x_j - a\Delta t = x_{j_0} + \alpha\Delta x,\ j_0 \in \mathbb{Z}, \alpha \in [0,1[$. The boundaries are treated as follows:

- the *inflow* side, corresponding to $x = -1$, relies on the analytical solution $f(t,x) = 0\ \forall x \leqslant at$. Whenever the scheme needs a value f_j^n with $j < 0$, it may be exactly taken equal to 0.
- in the case $d > 0$, the Lagrange stencil may also need *outflow* values f_j^n with $j > J$. Such values may be determined by polynomial extrapolation. Let $k_b \in \mathbb{N}$, and let p be the unique polynomial of degree k_b interpolating (x_j, f_j^n) for $j \in [\![J - k_b, J]\!]$. The *outflow ghost points* will be defined by $f_j^n \coloneqq p(-1 + j\Delta x)\ \forall j > N$ (NC: j'aurais mis $f_j^n \coloneqq p(1 + j\Delta x)\ \forall j > 0$ ou alors $f_j^n \coloneqq p(-1 + j\Delta x)\ \forall j > J$). (NC: N'y a-t-il pas une relation entre k_b et d ?)

4 Numerical results

The semi-Lagrangian code is written in `C`; it uses subroutines (translated from Fortran) of the selalib library [1]. The code works in parallel using MPI. The finite difference scheme has been written in Julia.

4.1 1-species validation test case

We rely on the work of [MK20] to provide an analytical solution in a 1-species case. Consider the simplified stationary (NC: pourquoi 'stationary' ?) model describing the density of particles $f = f(t,x,v)$, and the potential $\varphi = \varphi(t,x)$:

$$\begin{cases} \partial_t f + v\partial_x f - \partial_x\varphi\partial_v f = 0, & (t,x,v) \in \mathbb{R}_*^+ \times]-1,1[\times\mathbb{R}, \quad (4.1a) \\ \partial_{xx}^2\varphi = \displaystyle\int_{v\in\mathbb{R}} f dv, & (t,x) \in \mathbb{R}^+ \times]-1,1[. \quad (4.1b) \end{cases}$$

The initial and boundary conditions are given by

$$\begin{cases} f(0,x,v) \coloneqq f^0(x,v), \quad f(t, x = \pm 1, \pm v < 0) = 0, & (4.2a) \\ \varphi(t,0) = \partial_x\varphi(t,0) = 0. & (4.2b) \end{cases}$$

This model may be seen as a particular case of the two-species Vlasov-Poisson (2.2), upon taking the following parameters:

$$f_i^0 \equiv 0, \quad \nu = 0, \quad \mu = -1, \quad \lambda = 1, \quad f_e^0 = f^0.$$

The reader may verify that (4.1) is solved in $\mathbb{R}^+ \times [-1,1] \times \mathbb{R}$ by the following stationary couple:

$$f(t,x,v) \coloneqq \begin{cases} \frac{1}{\pi}\left(1 - x^2 - v^2\right)^{-1/2} & \text{if } x^2 + v^2 < 1, \\ 0 & \text{otherwise,} \end{cases} \quad \text{and} \quad \varphi(t,x) \coloneqq \frac{x^2}{2}. \quad (4.3)$$

[1] `https://selalib.github.io/selalib.html`

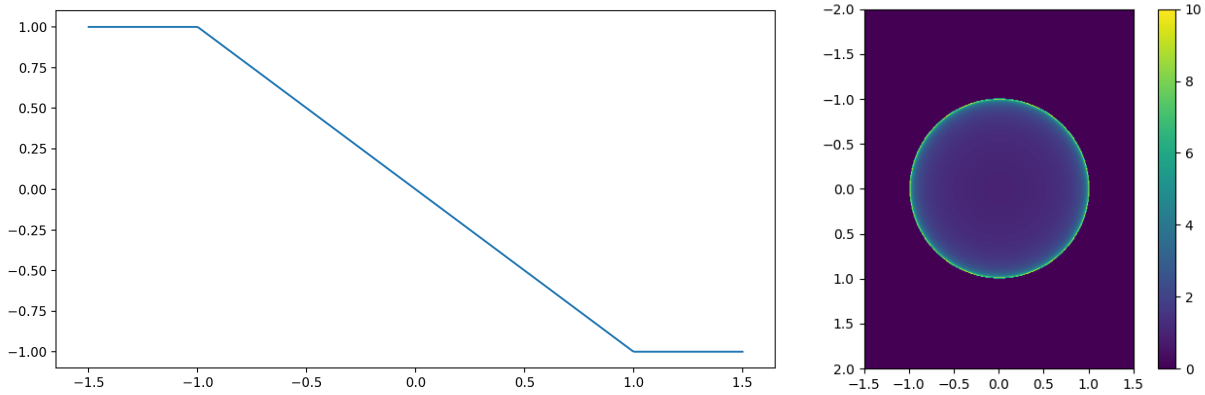

Figure 1: Malkov solutions (4.4) on $[-1.5, 1.5]$. Right: electric field E. Left: density f.

The electric field is extended outside of $[-1, 1]$ by a constant. The density f is represented in the domain $[-1.5, 1.5] \times [-2, 2]$, and truncated to 10.

It is numerically relevant to extend the Malkov solution (4.3) to spatial domains $x \in [-1-\varepsilon, 1+\varepsilon]$ by

$$f(t,x,v) := \begin{cases} \frac{1}{\pi}\left(1-x^2-v^2\right)^{-1/2} & \text{if } x^2+v^2<1 \\ 0 & \text{otherwise} \end{cases}, \quad \text{and} \quad \varphi(t,x) := \begin{cases} x^2/2, & x<1 \\ |x|-\frac{1}{2}, & x \geq 1 \end{cases} \tag{4.4}$$

Figure (1) illustrates the stationary solutions.
For now, I don't reach order 1. Maybe bug?

Parameters			Errors	
N_x	N_v	N_t	L^∞	L^1
100	2049	1281	8.59e-03	6.22e-03
200	2049	1281	1.22e-02	1.78e-02
400	2049	1281	6.22e-03	9.07e-03
800	2049	1281	7.13e-03	7.23e-03
100	4097	2561	5.65e-03	4.92e-03
200	4097	2561	3.88e-03	4.70e-03
400	4097	2561	4.08e-03	5.77e-03
800	4097	2561	2.39e-03	2.93e-03

Table 1: DF errors for Malkov test case.

Parameters			Errors	
N_x	N_v	N_t	L^∞	L^1
100	201	1000	1.30e-02	1.59e-03
200	401	1000	1.66e-02	1.88e-03
400	801	1000	1.88e-02	1.35e-03
800	1601	1000	6.15e-03	2.66e-04
100	101	100	3.19e-02	3.45e-03
200	201	200	2.77e-02	3.13e-03
400	401	400	6.49e-03	4.35e-04
800	801	800	1.51e-02	8.50e-04
1600	1601	1600	6.57e-03	2.50e-04
100	2049	10000	4.06e-03	4.62e-04
200	2049	10000	1.72e-02	1.40e-03
400	2049	10000	7.88e-03	3.90e-04
800	2049	10000	1.12e-02	5.37e-04
1000	201	5000	1.00e-02	3.32e-04
1000	401	5000	1.16e-02	5.48e-04
1000	801	5000	5.01e-03	1.72e-04
1000	1601	5000	6.34e-03	3.25e-04

Table 2: SL errors for Malkov test case.

4.2 Two species case

In this part, we focus on the two-species model (2.2) and n the sequel, we use the following physical parameters:

$$\lambda = \frac{1}{2}, \quad \mu = \frac{1}{100}, \quad \text{and} \quad \nu = 20. \tag{4.5}$$

The initial conditions are chosen as the thermodynamic equilibrium in an infinite spatial domain, or in a domain with periodic condition. The densities are then given by

$$f_i^0(x,v) \coloneqq \frac{\exp\left(-\frac{v^2}{2}\right)}{\sqrt{2\pi}}, \quad \text{and} \quad f_e^0(x,v) \coloneqq \sqrt{\mu}\frac{\exp\left(-\mu\frac{v^2}{2}\right)}{\sqrt{2\pi}}.$$

In order to satisfy the boundary conditions, we multiply $f_{i,e}$ by a mask, defined as

$$\text{mask}(x,v) \coloneqq \frac{1}{2}\left(\tanh\left(\frac{x-(-0.8)}{0.1}\right) - \tanh\left(\frac{x-0.8}{0.1}\right)\right).$$

Figure (2) illustrates the resulting initial conditions.

The simulations run over the spatial domain $x \in [-1,1]$. The semi-Lagrangian (SL) code computes the electron velocities on $v_e \in [-60,60]$, and ion velocities on $v_i \in [-50,50]$. The finite differences (FD) code uses the same mesh for ions and electrons, chosen as $v \in [-60,60]$. To simplify the comparison, visualisations of f_i are restricted to the coordinates $f_{i,j,k}$ such that $v_k \in [-5,5]$. For the finite differences code, we use $N_x = 512$, $N_{v_e} = N_{v_i} = 513$; the time step is computed in order to satisfy the CFL condition; a further time step is used for terminating to the final time T. For the semi-Lagrangian code, we will use

- Run0: $N_x = 512$, $N_{v_e} = N_{v_i} = 513$, $\Delta t = 0.00025$,
- Run1: $N_x = 256$, $N_{v_e} = 8193$ and $N_{v_i} = 2049$, $\Delta t = 0.00025$,
- Run2: $N_x = 1024$, $N_{v_e} = 8193$ and $N_{v_i} = 2049$, $\Delta t = 0.00025$,

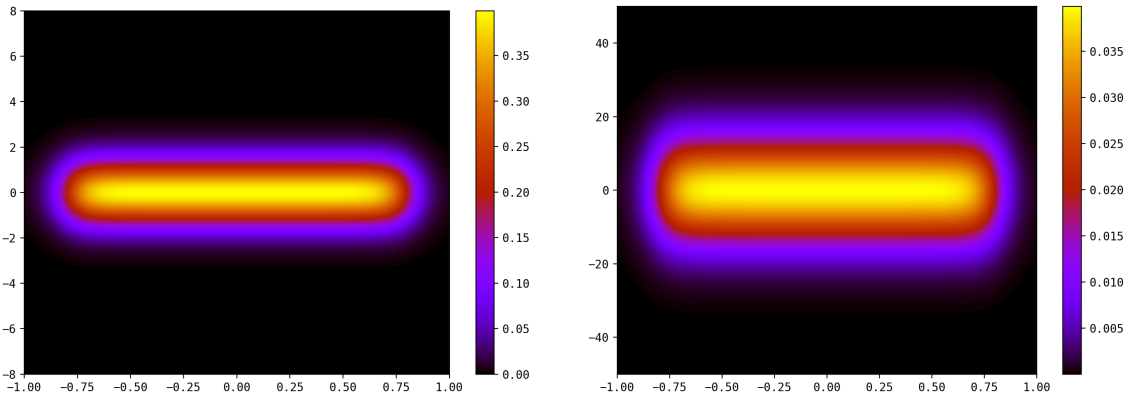

Figure 2: Initial conditions f_i^0 (left) and f_e^0 (right).

– Run3: $N_x = 1024$, $N_{v_e} = 8193$ and $N_{v_i} = 2049$, $\Delta t = 0.000025$.

Always for the SL scheme, we have used $d = 8$ with periodic boundary conditions for the interpolation in velocity, and $k_b = 1$ together with $d = 2$ for the spatial interpolation. Lagrange interpolation of degree 3 (that is, $d = 1$) is used for passing from the ion velocity mesh to the electron velocity mesh (which is needed for the ionization step).

As diagnostics, we represent the electric field E, the charge density $n = n_i - n_e$, the ion distribution function f_i and the electron distribution function f_e at different times $T \in \{0.1, 0.2, 1, 2, 5, 20\}$.

Short time We first look at the results for short times: $T = 0.1$ (Figure 3) and $T = 0.2$ (Figure 4). For the semi-Lagrangian code, we use the parameters of Run2, which gives a reference solution. We see that the results are very similar with the FD code for $T = 0.1$, which permits to validate the results by cross comparisons. For $T = 0.2$, differences begin to appear; the sharp profile of f_e is not well reproduced by the FD scheme which has also a coarser mesh. We can see also the differences on the charge density.

Long time Now, we turn to the long-term simulations, with $T = 20$, on Figure 5. The finite difference code suffers from numerical diffusion, and the approximations of f_i and f_e are much damped. Electric field and charge density are really different. On the contrary, the SL scheme gives much better results (in comparison with refined runs, as we will see later), while it uses the same number of points. We can distinguish a little degradation of the symmetry, by looking at the charge density.

Looking for a reference solution It is not easy to find a reference solution, as we look for long time solution, and the Vlasov equation is prone to filamentation. We have here also the problem that the time scale for the ions is different to the time scale for the electrons, which implies that short time steps have to be used in order to be able to follow the dynamics (even if we use here a semi-Lagrangian scheme, whose time step is not restricted by the strong CFL condition of the finite difference scheme).

It is interesting to notice that we can have converged solutions for a fixed time step, taking for exemple $\Delta t = 0.0025$ (or even $\Delta t = 0.025$), but the corresponding solution is then not (at all) converged in time (results are not shown here to save place; we can remark that the results on charge density can be quite different; looking at the electron distribution function, we see some shifting of the solution). So we have diminished the time step to $\Delta t = 0.00025$, and the comparison with the same simulations with $\Delta t = 0.000025$ on Figure 7 is now much similar, which indicates that the time step is now fine enough. Note that for semi-Lagrangian schemes, taking the smallest possible time step does not necessarily lead to a better result (due to accumulation of errors, as the number of interpolations increases).

We choose to use a very fine discretization in velocity for the electron by taking $N_v = 8193$ (some results, not shown, with $N_v = 16385$ have lead to indistinguishable results). We then make vary N_x and N_{v_i}; we remark that N_x can be quite lower and N_{v_i} a little lower also, as we have similar results taking $(N_x, N_{v_i}) = (256, 2049)$ and $(N_x, N_{v_i}) = (1024, 4097)$, as we can see on Figure 6 (the first one is more diffusive which is coherent).

We remark also that the spatial interpolation does not lead to unstable results, which can occur sometimes when extrapolation is used (see [BMN]). We have used an odd number of points in order to prevent from having 0 as mesh points, which would lead to increase of the value at constant rate, in the ionization step.

The study of the numerical equilibrium and the study of the behavior of the ion density around $(0, 0)$ which is quite complex at equilibrium, are not tackled here and are out of the scope of this work.

References

[Bad21] Mehdi Badsi. Collisional sheath solutions of a bi-species Vlasov-Poisson-Boltzmann boundary value problem. *Kinetic & Related Models*, 14(1):149, 2021.

[BBC21] Mehdi Badsi, Christophe Berthon, and Anaïs Crestetto. A stable fixed point method for the numerical simulation of a kinetic collisional sheath. *Journal of Computational Physics*, 429:109990, March 2021.

[BMG+] Emily Bourne, Yann Munschy, Virginie Grandgirard, Michel Mehrenberger, and Philippe Ghendrih. Non-Uniform Splines for Semi-Lagrangian Kinetic Simulations of the Plasma Sheath. page 35.

[BMN] Mehdi Badsi, Michel Mehrenberger, and Laurent Navoret. Numerical stability of plasma sheath. page 16.

[BNS+21] B. Boutin, T.H.T. Nguyen, A. Sylla, S. Tran-Tien, and J.-F. Coulombel. High order numerical schemes for transport equations on bounded domains. *ESAIM: Proceedings and Surveys*, 70:84–106, 2021.

[CL20] Jean-François Coulombel and Frédéric Lagoutière. The Neumann numerical boundary condition for transport equations. *Kinetic & Related Models*, 13(1):1–32, 2020.

[DPB16] Bruno Després, Martin Campos Pinto, and Mehdi Badsi. A minimization formulation of a bi-kinetic sheath. *Kinetic and Related Models*, 9(4):621–656, September 2016.

[MK20] Evgeny A. Malkov and Alexey N. Kudryavtsev. Non-stationary Antonov self-gravitating layer: Analytics and numerics. *Monthly Notices of the Royal Astronomical Society*, 491:3952–3966, January 2020.

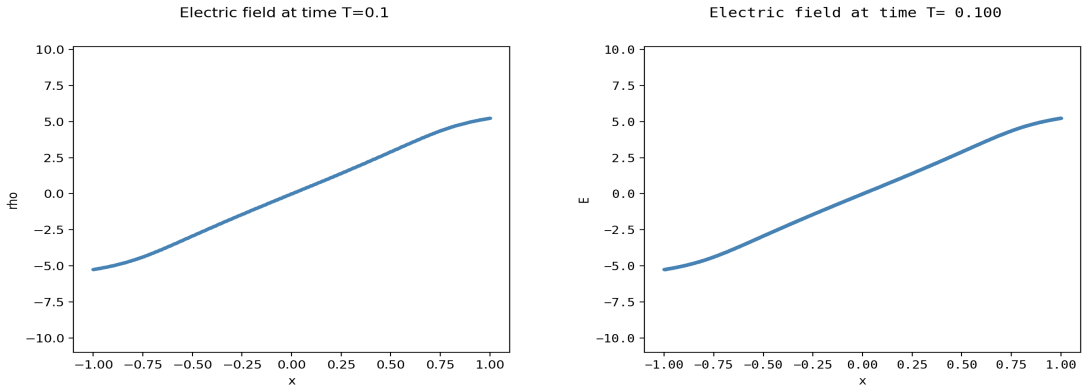

(a) Electric field

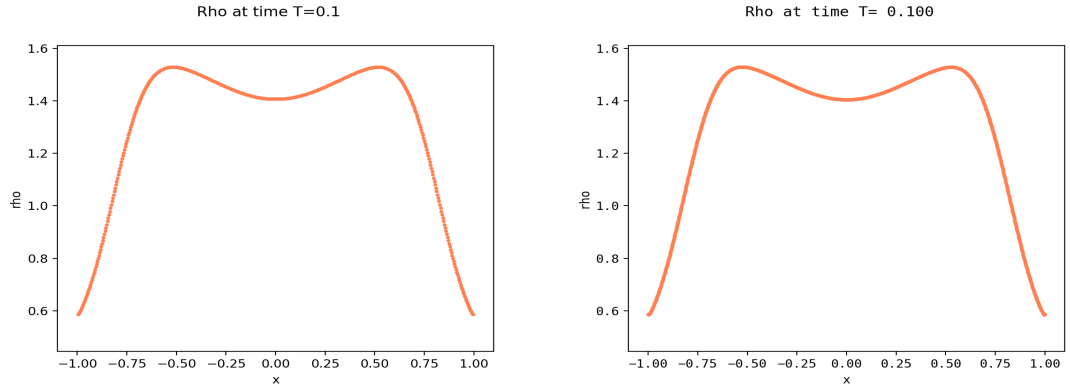

(b) Density ρ

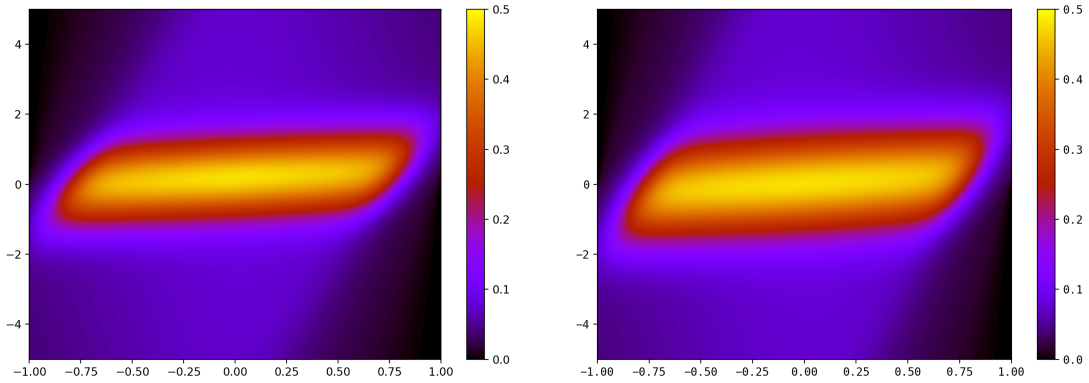

(c) Ion distribution function

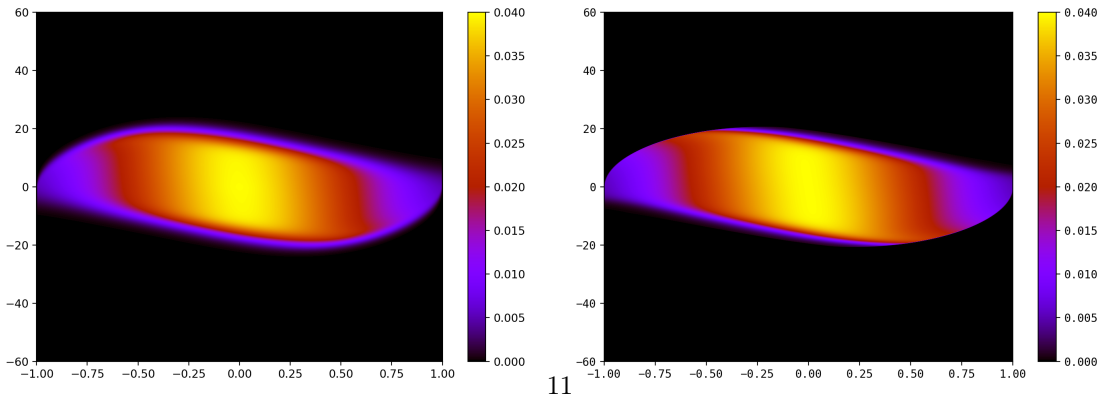

(d) Electron distribution function

Figure 3: Comparison between finite differences (left) and semi-Lagrangian (right) at $T = 0.1$. The Semi-Lagrangian code uses parameters of Run2

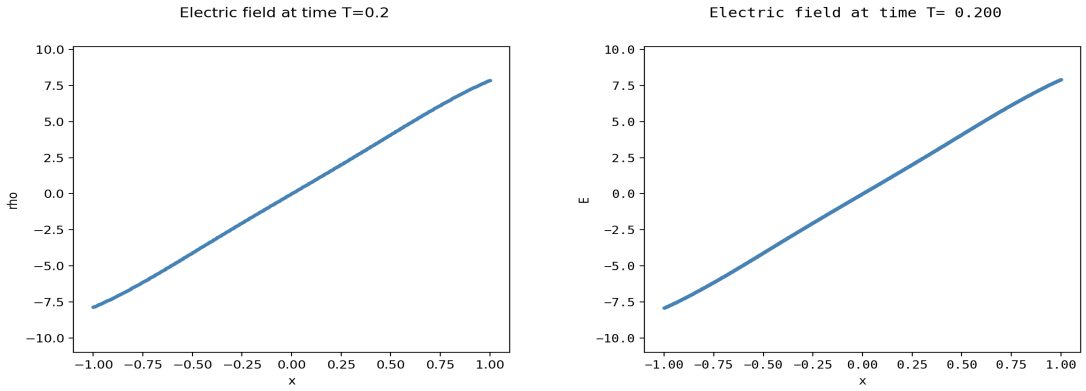

(a) Electric field

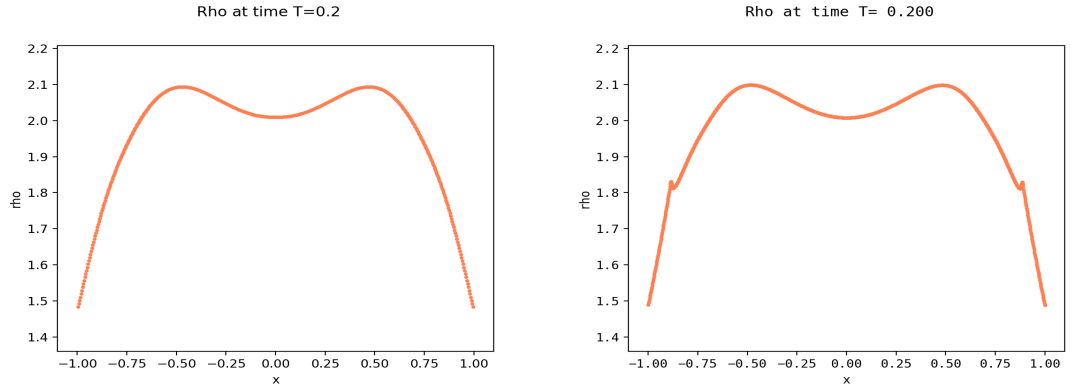

(b) Density ρ

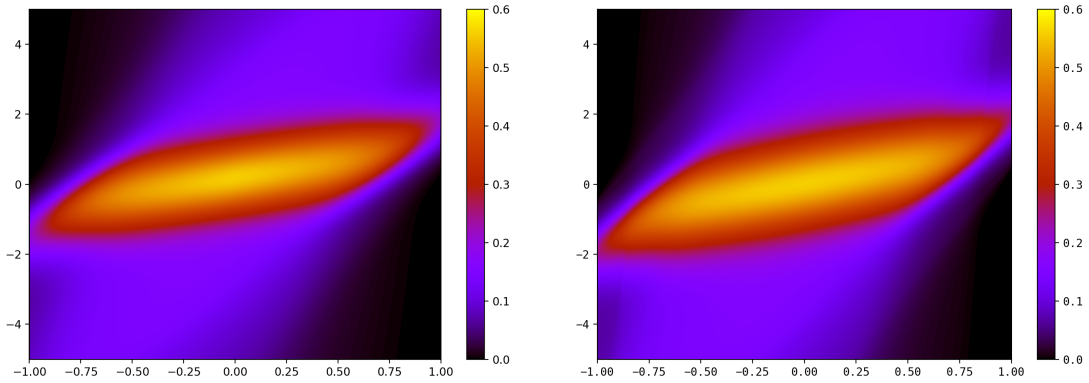

(c) Ion distribution function

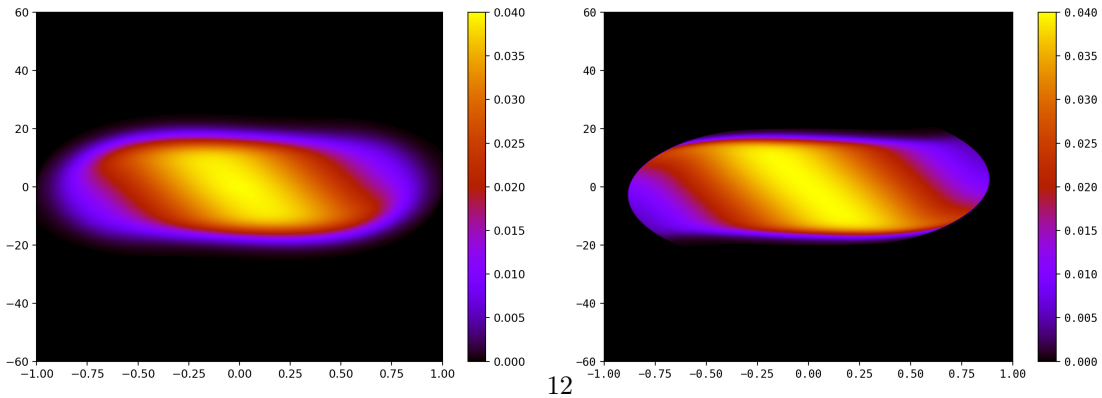

(d) Electron distribution function

Figure 4: Comparison between finite differences (left) and semi-Lagrangian (right) at $T = 0.2$. The Semi-Lagrangian code uses parameters of Run2

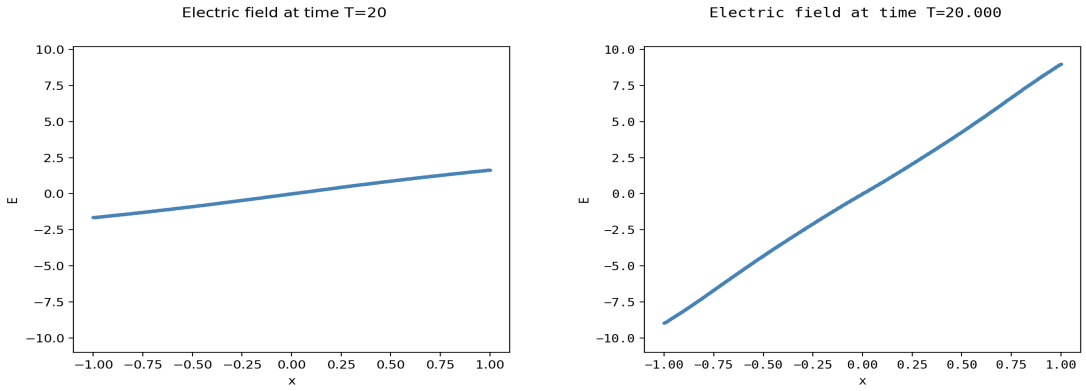

(a) Electric field

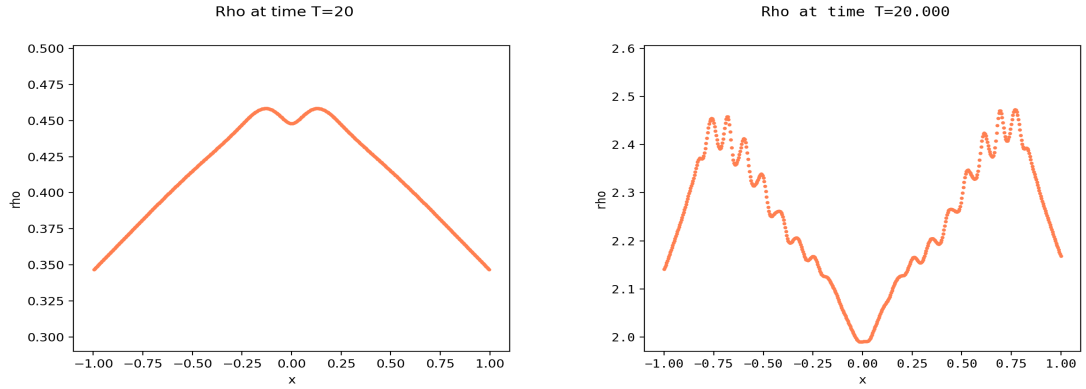

(b) Density ρ

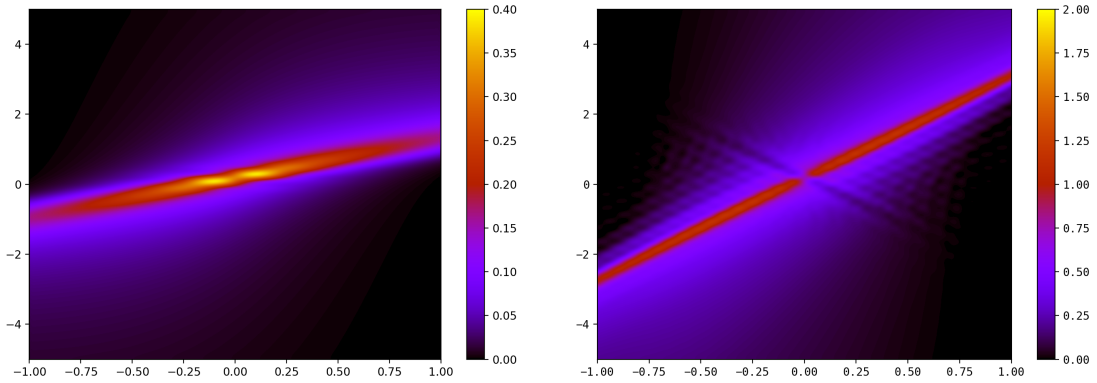

(c) Ion distribution function

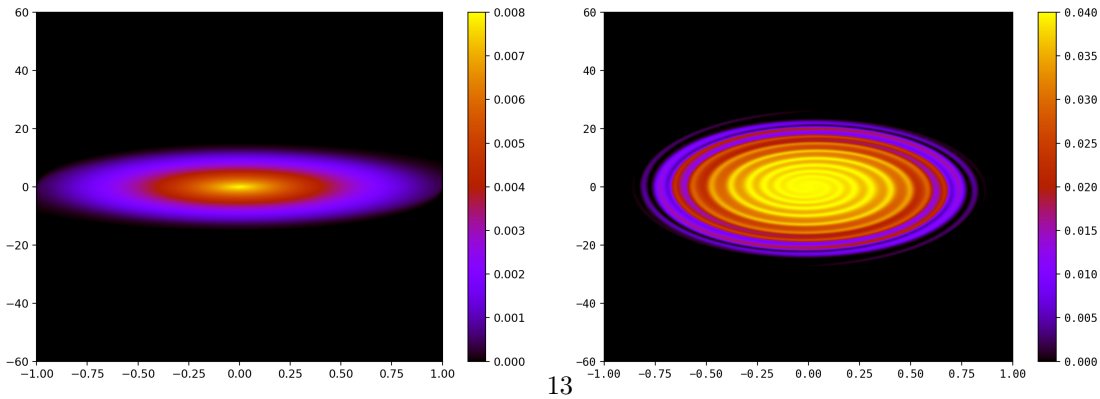

(d) Electron distribution function

Figure 5: Comparison between finite differences (left) and semi-Lagrangian (right) at $T = 20$. The Semi-Lagrangian code uses parameters of Run0

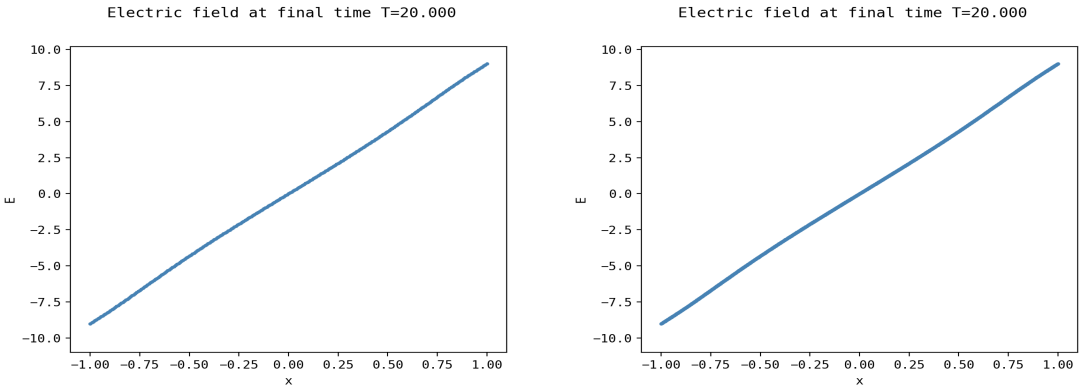

(a) Electric field

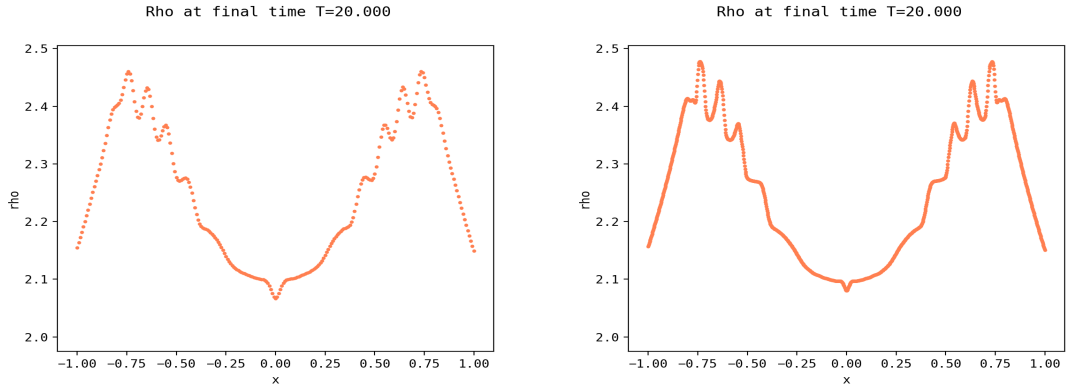

(b) Density ρ

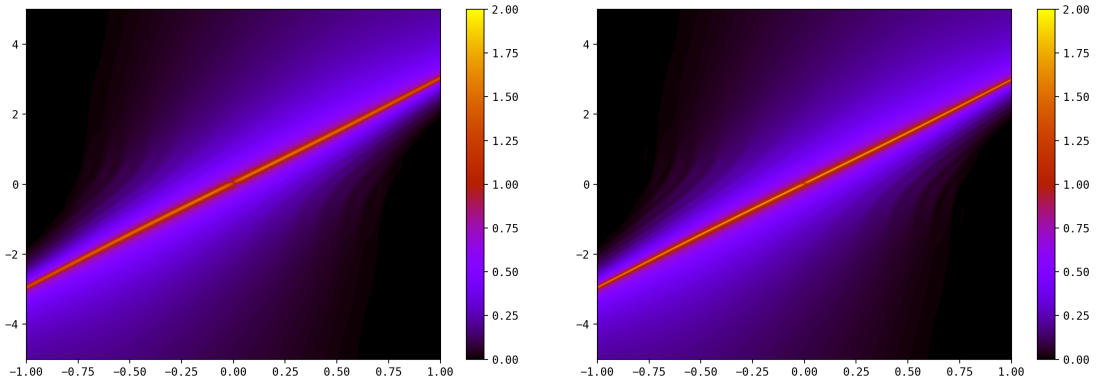

(c) Ion distribution function

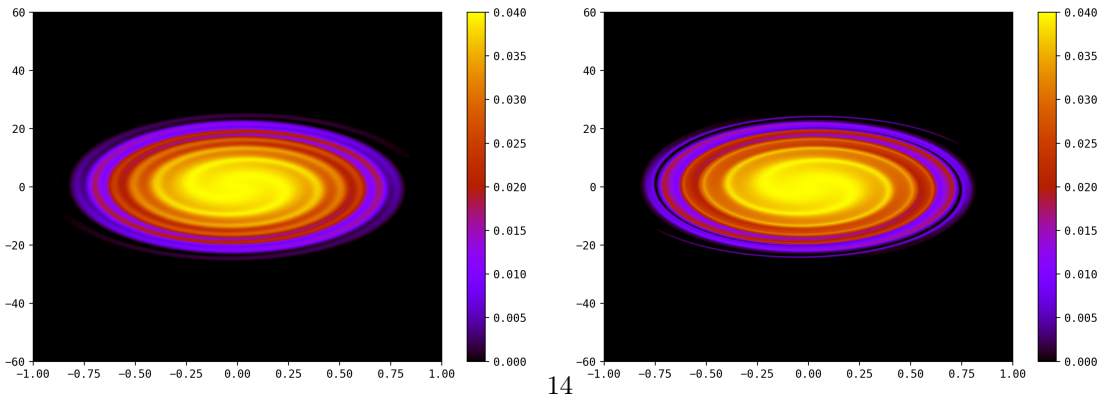

(d) Electron distribution function

Figure 6: Comparison of semi-Lagrangian codes: parameter of Run1 (left) and parameters of Run2 (right)

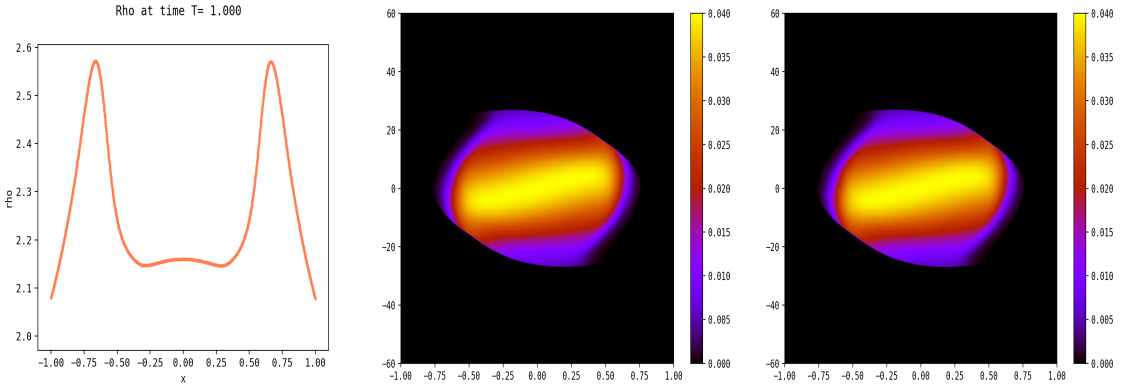

(a) $T = 1$

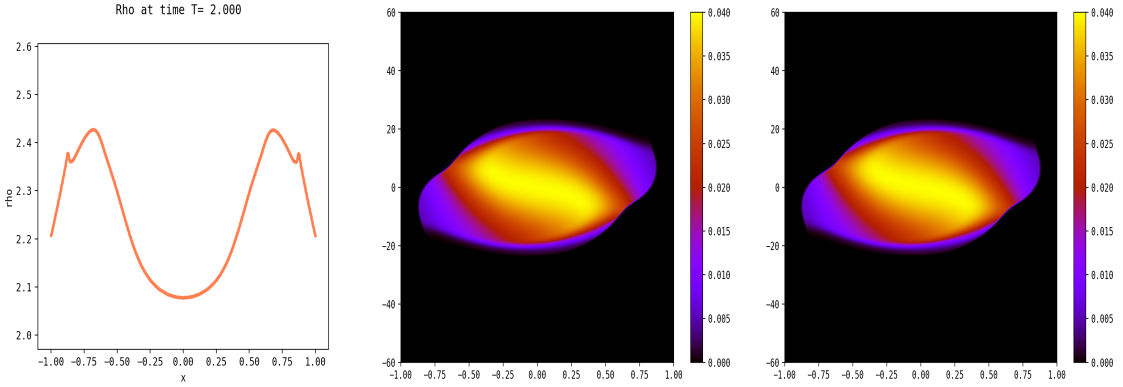

(b) $T = 2$

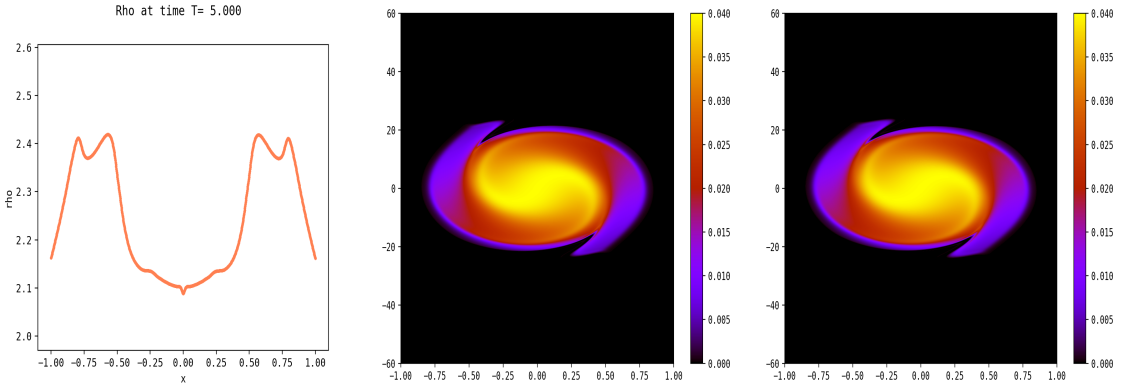

(c) $T = 5$

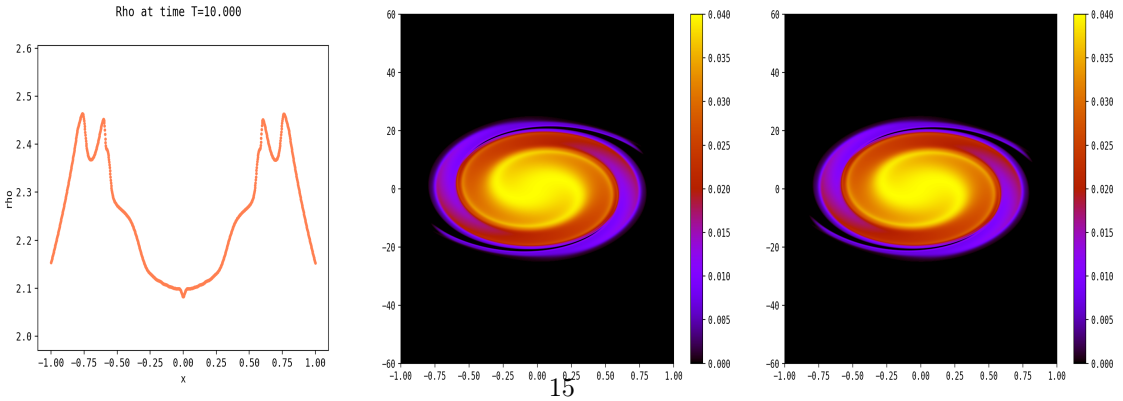

(d) $T = 10$

Figure 7: Density ρ (left) and electron distribution function (middle and right) for time $T \in \{1, 2, 5, 10\}$; The Semi-Lagrangian code is used with parameters of Run2 (left, middle) and of Run3 (right).